Int. J. Heat Mass Transfer. Vol. 9, pp. 1167–1187. Pergamon Press 1966. Printed in Great Britain

THE LEIDENFROST PHENOMENON: FILM BOILING OF LIQUID DROPLETS ON A FLAT PLATE

B. S. GOTTFRIED*, C. J. LEE† and K. J. BELL‡

(*Received* 30 *August* 1965 *and in revised form* 11 *January* 1966)

Abstract—The film boiling of small droplets of liquid on a hot flat surface in the atmosphere is commonly termed the Leidenfrost Phenomenon after J. G. Leidenfrost who first studied the process in 1756.

In the present study, the total evaporation times were determined for small droplets (<0·1 ml) of water, carbon tetrachloride, ethanol, benzene, and *n*-octane on a stainless steel plate at surface temperatures ranging from 150°C to 500°C. Most of the data were taken in the film boiling regime though data were also taken in the nucleate and transition boiling regimes. The Leidenfrost point, defined as the plate temperature at which the droplet evaporation time is greatest, was determined. The Leidenfrost point was found to be 100–105 degC above the saturation temperature for all liquids except water; for water, the exact value of the Leidenfrost point appears to depend upon the surface and the method of depositing the droplet and varies from 150 degC to 210 degC above saturation. The Leidenfrost point is independent of droplet size over the range studied.

An analytical model of the Leidenfrost phenomenon is postulated: Heat is transferred to the droplet by conduction through the vapor film on the bottom half and by radiation to the entire droplet. Mass is removed from the droplet by evaporation on the lower surface to supply the vapor film and by diffusion from the upper surface. The droplet is supported by the excess pressure in the vapor film. The droplet is presumed spherical and isothermal at the saturation temperature. The instantaneous evaporation rate is found by satisfying the heat, mass, and momentum balances for this model; total evaporation times are calculated by integrating the evaporation rate. Calculated and experimental evaporation times agree within 20 per cent except for *n*-octane at high temperatures, where some thermal cracking may have occurred.

NOMENCLATURE

A_1, surface area of lower half droplet [cm^2];

A_2, surface area of upper half droplet [cm^2];

A_p, projected area of liquid droplet [cm^2];

A_s, area of stainless steel plate [cm^2];

C_1, C_2, correlational constants from experimental data [dimensionless];

C_p, mean specific heat of vapor [cal/g degC];

D, molecular diffusion coefficient for vapor in air [cm^2/s];

F, total upward force exerted on droplet [dynes];

$\bar{F}_1, \bar{F}_2$, configuration factor for radiation between hot plate and droplet [dimensionless];

$\mathscr{F}_1, \mathscr{F}_2$, overall configuration factors for radiation between hot plate and droplet [dimensionless];

g, gravitational acceleration [cm/s^2];

$I_1(\delta_1/r, \theta')$, integral defined in equation (19);

$I_2(\delta_1/r, \theta'')$, double integral defined in equation (18);

* Department of Mechanical Engineering, Carnegie Institute of Technology, Pittsburgh, Pennsylvania.

† Research Center, Phillips Petroleum Company, Bartlesville, Oklahoma.

‡ School of Chemical Engineering, Oklahoma State University, Stillwater, Oklahoma.

$I_3(\delta_1/r)$, triple integral defined in equation (17);
K, correction factor defined as $k(1+K) = k_e$ [dimensionless];
k, thermal conductivity of vapor at T_V [cal/s cm degC];
k_c, mass-transfer coefficient based on concentration [cm/s];
k_e, effective thermal conductivity as defined in equation (14) [cal/s cm degC];
M, molecular weight of vapor [g/g-mole];
P, excess pressure beneath droplet [dyne/cm^2];
$P(\theta'')$, excess pressure at angular position θ'' [dyne/cm^2];
P_s, partial pressure of the diffusing vapor [dyne/cm^2 or atm];
Q_c, total heat conducted through the vapor film generated on bottom of droplet [cal/s];
Q_{R1}, net radiation from plate to lower half of droplet [cal/s];
Q_{R2}, net radiation from plate to upper half of droplet [cal/s];
q_c, conductive-convective heat flux through the vapor film [cal/s cm^2];
r, radius of droplet at any time [cm];
r_0, initial radius of droplet [cm];
T_P, plate temperature [°K];
T_S, saturation temperature of liquid droplet [°K];
T_V, mean vapor temperature beneath droplet [°C];
ΔT, $T_P - T_S$ [degC];
t, time [s];
u, radial vapor velocity beneath droplet [cm/s];
$\bar{u}$, mean radial vapor velocity beneath droplet [cm/s];
V, droplet volume [cm^3];
W_1, rate of evaporation over lower half of droplet [g/s];
W_2, rate of evaporation over upper half of droplet [g/s];
x, radial space variable beneath droplet [cm];
y, axial space variable beneath droplet [cm].

Greek symbols

δ, vertical distance from some point on lower droplet surface to plate [cm];
δ_1, vertical distance from bottom center of droplet to plate [cm];
$\bar{\delta}$, mean vapor film thickness beneath droplet [cm];
ε_L, thermal emissivity of liquid [dimensionless];
ε_P, thermal emissivity of stainless steel [dimensionless];
λ, heat of vaporization of saturated liquid [cal/g];
λ', $= \lambda + (\Delta T/2)\, C_p$ [cal/g];
μ, viscosity of vapor at T_V [g/cm s];
ρ_L, density of saturated liquid [g/cm^3];
ρ_V, density of vapor [g/cm^3];
σ, Stefan–Boltzmann constant, $1{\cdot}355 \times 10^{-12}$ [cal/(degK)^4 cm^2 s];
$\bar{\sigma}$, surface tension liquid [dyne/cm];
τ, total droplet evaporation time [s];
θ, angular variable in droplet [rad];
θ', θ'', dummy angular variables in droplet [rad].

1. INTRODUCTION

THE LEIDENFROST PHENOMENON is the term traditionally given to the body of phenomena observed when small amounts of liquid are placed or spilled on a very hot surface. The Phenomenon is frequently if inadvertently provoked in the kitchen by spilling water on a hot

frying pan; one may note the presence of large and small masses moving rapidly about the surface without wetting it, the dancing of small droplets, the disruption of larger masses by bubbles breaking through, hissing and spitting when liquid contacts a cooler surface, and withal, the relative slowness of evaporation. From the presence of many tiny spheroids, the Phenomenon is often termed the Spheroidal State. This name invites and has caused confusion with a number of unrelated processes and we will not use it further.

The chief features of the Phenomenon were first carefully studied and reported in 1756 by Johann Gottlob Leidenfrost [1], after whom the Phenomenon was subsequently named. Leidenfrost's treatise has been translated out of the original Latin into English for the first time (to the best knowledge of the present authors) by Mrs. Carolyn Wares of the University of Oklahoma [2]. This treatise is often cited (presumably by those who have read it in the original) as the first substantial study of boiling heat transfer.

The definitive experiments reported by Leidenfrost are on the evaporation of quiescent, relatively small masses of liquid resting on a spoon at temperatures up to red heat; the present study covers essentially the same area. Leidenfrost's evaporation rate data were limited in number and led him to believe that evaporation time for a given drop size increased monotonically with surface temperature (cf. Fig. 7 of the present paper). The difficulty arose from his inability to measure high temperatures. Leidenfrost turned this to an advantage and proposed using droplet evaporation time to measure surface temperatures—a good idea, but falsely predicated. It is evident that Leidenfrost did not realize that he was conducting a boiling experiment—boiling for him meant nucleate boiling; indeed, he refers to the droplet becoming more "fixed"—i.e. rigid or stable—in the fire.

Leidenfrost makes particular note that a small solid deposit was occasionally left behind on the spoon—usually after an evaporation requiring a long period of time. We presume this is due to dust in the laboratory; we encountered this difficulty too. But Leidenfrost, in an intellectual environment that still had room for Aristotle's Four Elements, at least entertained the possibility that he had observed here the reaction: Fire + Water → Earth.

In evaluating Leidenfrost's work, it is well to remember that, at that date, the latent heat of phase transformation was an unknown concept; heat and cold were considered different fluids (unless they were calorific and frigorific rays); and air, gases and vapors were poorly distinguished if at all.

Many researchers after Leidenfrost studied the Phenomenon. Over 40 original references are known to the authors and they form an interesting sequence in the growth (not always forward) of comprehension. Only a few key references will be discussed here in the expectation that the entire literature will be examined in a separate publication later.

Rumford [3] believed that a stratum of air adhered strongly to the metal surface, even beneath the drop; the poor conductance of heat through the air layer accounted for the slow evaporation. He was aware that heat conducted to the droplet supplied the latent heat of vaporization.

Poggendorff [4] first showed that a quiescent droplet was separated from the plate by an electrical insulator; Stark [5] among others later showed that a bouncing droplet would occasionally complete an electrical circuit with the plate and hence presumably touched the plate.

Boutigny [6] performed several experiments on the Leidenfrost Phenomenon (to which he gave the name "Spheroidal State" for the first time), one of which clearly established that the total evaporation time decreased as surface temperature increased above the minimum for existence of the Leidenfrost Phenomenon. He also reported some liquid temperatures for large masses (12–15 ml) of water in a hemispherical silver container over a lamp. His thermo-

meter showed temperatures ranging from 96·5°C to 102°C; repeating the experiment with other liquids, he found that the *bulk* of the mass was always a few degrees below saturation. This was mistakenly interpreted by several authors (up to and including Partington [7]) as implying that the liquid is *nowhere* at its boiling temperature, and therefore some other mechanism than boiling must be considered to be responsible for the Leidenfrost Phenomenon. In fact, Boutigny's results are just what the authors would expect from the model proposed in this paper. At that time Boutigny's work does not seem to have caused any confusion and the qualitative description and explanation of the Phenomenon given by Gmelin [8] in 1848 cannot be improved upon by the present authors.

However, by 1863, at least two theories not involving boiling were current [9]. In one, the radiant heat is presumed to push the droplet away from the surface; in the other, the adhesive force between the liquid and surface was presumed to be so weakened by heat that the liquid would be drawn to itself by cohesion and the small balls thus formed would evaporate slowly into the surrounding hot gas. Certain parts of the second theory have been incorporated into the present model. The first theory eventually developed into a thermal diffusion model which persisted until (hopefully) Kistemaker [10] laid it to rest in 1963 by showing that the thermal diffusion effect is several orders of magnitude too small to support the droplet. Berger [9] showed by a large number of experiments that the alternative theories to film boiling were not essential, but he did not disprove them. His experiments suggested that the Leidenfrost Phenomenon could be evoked with any liquid on any surface if the liquid could be made to boil without decomposing and the surface could be heated strongly enough.

The first attempt at a semianalytical solution of the Leidenfrost Phenomenon appears to be due to Pleteneva and Rebinder [11] in 1946. Their treatment relies upon experimental data to evaluate a constant and is not in any sense an analysis of the mechanisms of heat, mass, and momentum transport. They establish the Leidenfrost temperature for a number of liquids and calculate that the mean vapor film thickness beneath the droplet is about 0·009 cm for water, methanol, and benzene.

Borishansky [12] proposed a dimensional analysis for the correlation of vaporization time for small droplets. To generate the pertinent dimensionless correlating groups, he wrote a heat continuity differential equation at the vapor–liquid interface and a differential heat balance equation on the droplet. The final correlation of experimental data is shown as a graph in the paper. It is important to note that the fluid dynamics of the vapor and diffusion mass transfer were not considered, no force balance was made and in the final analysis radiation was omitted as negligible.

Also in 1953, Gorton [13] postulated an analytical model based on potential flow of the vapor; this is apparently the first treatment from first principles of the Phenomenon. However, present studies suggest that the vapor flow is laminar rather than potential. Gorton's experiments were made using a steady-state droplet suspended from a syringe, and the supporting force due to the surface tension between droplet and syringe belies the force balance. The attempt to photographically measure the vapor thickness failed.

Kistemaker [10] in 1963 reported some work done much earlier and used essentially the same experimental technique as Gorton. However, Kistemaker used X-rays with a barium-loaded water droplet to measure the vapor thickness and obtained a mean value of 0·006 cm for a 0·05-ml water droplet at 500°C plate temperature. Kistemaker also attempted an analytical treatment starting with the Navier–Stokes equation for vapor flow underneath the droplet. Unfortunately, there is an error in his analysis which causes the viscosity-dependent terms to cancel out, leaving a potential flow like that assumed by Gorton.

In 1962, Gottfried [14] studied the Leiden-

frost problem with the intent of achieving a complete mechanistic analysis of the problem with as few assumptions as reasonable. Gottfried was able to predict droplet vaporization times to within a maximum error of 25 per cent; however, the final result incorporated one experimentally-determined "universal" constant, and the present work is an attempt to remove that empiricism and to provide additional data to test the model.

The present paper is confined to (1) an experimental investigation of the behavior and especially the evaporation rate of small (nearly spheroidal) droplets on a hot flat surface with no evident bouncing, spitting or hissing, and (2) development of an analytical model to predict evaporation rate of droplets under these conditions. The authors presume in the following discussion that the essential mechanism of the Leidenfrost Phenomenon is the film boiling of a liquid phase whose quantity is insufficient to completely cover the heating surface. The liquid exists in small masses separated from the surface by a film of vapor generated by vaporization of the liquid. The masses are supported by the pressure gradient in the vapor flowing underneath the mass. Other mechanisms have been proposed in the past and will be described later in this section. In a later paper, the authors will deal with the problem of larger masses in which some of the vapor escapes by breaking through the mass as bubbles rather than escaping to the outer edge.

2. THEORETICAL DEVELOPMENT

It is postulated that several physical processes occur simultaneously over the upper and lower surfaces of the droplet. Heat is transferred to the droplet by conduction through the (moving) vapor film between the lower half of the droplet and the hot surface and by radiation from the hot surface to the entire outer surface of the droplet. Mass is removed from the droplet by evaporation into the vapor film on the lower surface and by diffusion-controlled evaporation on the upper half surface. A radial pressure gradient in the vapor film causes it to flow and the integrated product of the pressure (above atmospheric) and the horizontal projection of the lower drop surface supports the droplet.

The corresponding mass, heat, momentum, and force balances must be satisfied. To write the necessary equations, the droplet is assumed spherical and isothermal at its saturation temperature. The vapor in the film between droplet and plate is assumed to be superheated to a temperature halfway between saturation and the plate surface temperature. Figure 1 diagrams the processes. Q_c is the heat conducted to the

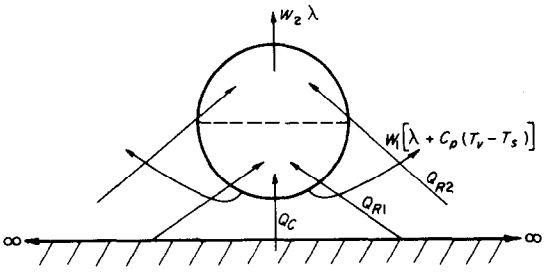

FIG. 1. Heat-transfer and mass-transfer paths for the spherical droplet model

droplet, Q_{R1} is the net heat radiated to the lower surface, and Q_{R2} is the net heat radiated to the upper surface. W_1 is the overall rate of evaporation on the lower surface, and W_2 the rate on the upper surface. By a mass balance

$$\rho_L \frac{dV}{dt} = -(W_1 + W_2) \tag{1}$$

and by a heat balance

$$Q_c + Q_{R1} + Q_{R2} = W_1[\lambda + C_p(T_V - T_S)] + W_2\lambda. \tag{2}$$

The mass loss rate from the upper surface W_2 may be explicitly calculated. Assume that the removal process is pure molecular diffusion; then

$$W_2 = \frac{k_c M P_s}{RT_S} A_2 = \frac{DMP_s A_2}{RT_S r} \tag{3}$$

where $P_s = 1$ atm for the present work.

Momentum balance considerations enter into the analysis on the lower half of the droplet. If we assume that:

(1) The variation of velocity with time is small compared to the variation with respect to spatial coordinates,
(2) The internal terms are small compared to viscous terms (i.e. low vapor Reynolds number),
(3) The flow channel is very narrow compared to its length,

then the Navier–Stokes equations in cylindrical coordinates simplify to

$$\frac{\partial P}{\partial x} = \mu \frac{\partial^2 u}{\partial y^2}. \tag{4}$$

These assumptions are plausible in the light of actual values developed later. Assuming no slip at the vapor boundaries, equation (4) may be integrated to

$$u = \frac{1}{2\mu} \frac{\partial P}{\partial x}(y - \delta)y. \tag{5}$$

Now consider a cylinder of height δ and radius x, $0 \leqslant x \leqslant r$, of an incompressible fluid (see Fig. 2). A material balance may be written as

$$W_1(\theta') = \rho_V 2\pi x \delta \bar{u} \tag{6}$$

where $\bar{u}$ is the average radial velocity of the vapor at θ' defined by

$$\bar{u} = \frac{1}{\delta}\int_0^{\delta} u \, dy = \frac{\delta^2}{12\mu}\left(-\frac{\partial P}{\partial x}\right). \tag{7}$$

Introducing equation (7) into (6), and making θ' the variable of integration, the pressure distribution in the vapor stream is given by

$$\int_{P(0)}^{P(\theta'')} (-dP) = \frac{6\mu}{\pi\rho_V}\int_0^{\theta''} \frac{W_1(\theta')\cos\theta' \, d\theta'}{\sin\theta'[\delta_1 + r - r\cos\theta']^3} \tag{8}$$

where $P(\theta'')$ is defined as the excess pressure existing beneath the droplet and $P(0)$ is the excess pressure exerted at the bottom center of the droplet. $P(\theta'')$ vanishes at $\theta'' = \pi/2$; therefore,

$$P(0) = \frac{6\mu}{\pi\rho_V}\int_0^{\pi/2} \frac{W_1(\theta')\cos\theta' \, d\theta'}{\sin\theta'[\delta_1 + r - r\cos\theta']^3} \tag{9}$$

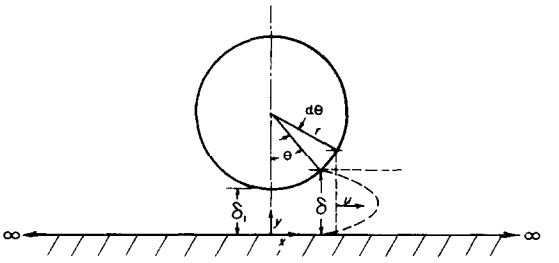

FIG. 2. Geometric configuration for the spherical droplet model.

Some geometric relationships:

$$\delta = \delta_1 + r(1 - \cos\theta)$$
$$x = r\sin\theta$$
$$dx = r\cos\theta \, d\theta$$
$$dA_p = 2\pi x \, dx = 2\pi r^2 \sin\theta\cos\theta \, d\theta.$$

The pressure at any given point on the lower surface from equation (8) and (9) is

$$P(\theta'') = \frac{6\mu}{\pi\rho_V}\int_{\theta''}^{\pi/2} \frac{W_1(\theta')\cos\theta' \, d\theta'}{\sin\theta'[\delta_1 + r - r\cos\theta']^3}. \tag{10}$$

The total upward force which is exerted on the droplet is

$$F = \int_{A_p} P(\theta'') \, dA_p = 2\pi r^2 \int_0^{\pi/2} P(\theta'')\sin\theta''\cos\theta'' \, d\theta''. \tag{11}$$

Since the liquid droplet is assumed quiescent on the hot plate, this excess force acting on the droplet from underneath must be counterbalanced by the weight of the droplet, i.e.

$$\tfrac{4}{3}\pi r^3(\rho_L - \rho_V)g = 2\pi r^2 \int_0^{\pi/2} P(\theta'')\sin\theta''\cos\theta'' \, d\theta''. \tag{12}$$

Introducing equation (10) into equation (12)

and rearranging

$$r = \frac{q}{\pi} \frac{\mu}{g\rho_V(\rho_L - \rho_V)} \int_0^{\pi/2} \sin\theta'' \cos\theta'' \, d\theta'' \int_{\theta''}^{\pi/2} \frac{W_1(\theta') \cos\theta' \, d\theta'}{\sin\theta'[\delta_1 + r - r\cos\theta']^3}. \quad (13)$$

The local rate of vapor generation over the lower surface of the droplet, $W_1(\theta')$, appears implicitly in equation (13). The solution of this equation therefore requires hypothesizing the mechanisms of heat and mass transfer taking place on the lower portion of the droplet.

Assume that the vapor generation from the bottom of the droplet up to a position θ', $W_1(\theta')$, is due to an *effective* heat conduction in the y-direction from the heating plate to the droplet, i.e.

$$d[W_1(\theta')] = \frac{1}{\lambda'}\left[\frac{k_e \Delta T}{\delta}\right] dA_p \quad (14)$$

or

$$W_1(\theta') = \frac{2\pi r k_e \Delta T}{\lambda'} \int_0^{\theta'} \frac{\sin\theta\cos\theta \, d\theta}{[\delta_1/r + 1 - \cos\theta]} \quad (15)$$

where λ' is the heat of vaporization with the superheating being taken into consideration.

The symbol k_e in equation (15) denotes the effective thermal conductivity for the hypothetical heat conduction mechanism including a correction for radiation effects described later.

Introducing equation (15) into (13) gives

$$r^3 = \frac{18\mu k_e \Delta T}{g\rho_V(\rho_L - \rho_V)\lambda'} I_3(\delta_1/r) \quad (16)$$

where

$$I_3(\delta_1/r) = \int_0^{\pi/2} \sin\theta'' \cos\theta'' \, I_2(\delta_1/r, \theta'') \, d\theta'' \quad (17)$$

where

$$I_2(\delta_1/r, \theta'') = \int_{\theta''}^{\pi/2} \frac{\cos\theta' \, I_1(\delta_1/r, \theta') \, d\theta'}{\sin\theta'[\delta_1/r + 1 - \cos\theta']^3} \quad (18)$$

and where

$$I_1(\delta_1/r, \theta') = \int_0^{\theta'} \frac{\sin\theta\cos\theta \, d\theta}{\delta_1/r + 1 - \cos\theta}. \quad (19)$$

In use, these integrals were first evaluated numerically and the results curve-fitted for faster computation in the main program.

Finally the total evaporation rate from the lower half of the droplet is

$$W_1 = W_1(\theta' = \pi/2) = \frac{2\pi r k_e \Delta T}{\lambda'} I_1(\delta_1/r, \pi/2). \quad (20)$$

We now proceed to evaluate k_e, taking account of both conduction and radiation. We emphasize that the overall heat and mass balances must be maintained, so one cannot arbitrarily say that

$$Q_c + Q_{R1} = W_1[\lambda + C_p(T_V - T_S)].$$

It is observed in fact that the droplet is internally mixed and nearly isothermal; therefore, heat is transferred between top and bottom halves of the droplet in an amount corresponding to the subcooling and the mixing rate.

Let q_c be the heat-transfer rate per unit area due to thermal conduction through the vapor film existing between the plate and bottom of the droplet. If we assume that conduction is in the y direction only, the Fourier equation gives

$$q_c = \frac{k \Delta T}{\delta}$$

or

$$Q_c = \int_{A_p} \frac{k \Delta T}{\delta} dA_p = \frac{k \Delta T}{\bar{\delta}} A_p \quad (21)$$

where $\bar{\delta}$ is the mean film thickness through which heat is conducted from the heating surface to the liquid droplet. By substituting the geometrical relationships of Fig. 2 into equation (21)

$$\bar{\delta} = \left[\frac{2(\delta_1 + r)}{r^2} \ln\frac{\delta_1 + r}{\delta_1} - \frac{2}{r}\right]^{-1}. \quad (22)$$

The heat-transfer rate due to thermal conduction from the heating surface to the droplet, therefore, can be expressed by equations (21) and (22).

Radiative heat transport becomes more important as the plate temperature increases. Assuming that the plate and the lower half of the droplet are separated by a non-absorbing, non-emitting medium, the rate of radiative heat transfer between these two bodies is given by reference [15].

$$Q_{R1} = A_1 \mathscr{F}_1 \sigma (T_P^4 - T_S^4) \tag{23}$$

where $\mathscr{F}_1$ is the overall interchange factor for radiation between the hot plate and the lower half of the liquid droplet. $\mathscr{F}_1$ is given for a system of two-zone, source-sink surfaces in reference [15]:

$$\frac{1}{\mathscr{F}_1} = \left(\frac{1}{\varepsilon_L} - 1\right) + \frac{A_1}{A_S}\left(\frac{1}{\varepsilon_R} - 1\right) + \frac{1}{\bar{F}_1}. \tag{24}$$

Since $A_1 \ll A_s$, equation (24) can be further simplified to

$$\frac{1}{\mathscr{F}_1} = \left(\frac{1}{\varepsilon_L} - 1\right) + \frac{1}{\bar{F}_1}. \tag{25}$$

Similarly, the overall interchange factor for radiation between the plate and the upper half of the liquid droplet is

$$\frac{1}{\mathscr{F}_2} = \left(\frac{1}{\varepsilon_L} - 1\right) + \frac{1}{\bar{F}_2} \tag{26}$$

$\bar{F}_1$ and $\bar{F}_2$ are the average configuration factors for radiation between the lower and upper halves of the spherical droplet and the plate respectively. The pointwise configuration factor is $F(\theta_1) = (2\pi - 2\theta_1)/2\pi$; the average configuration factor is (see Fig. 3)

$$\bar{F}_1 = \frac{\int_{A_1} F(\theta_1)\,\mathrm{d}A_1}{A_1} =$$

$$= \frac{1}{2\pi r^2}\int_0^{\pi/2}\left(\frac{2\pi - 2\theta_1}{2\pi}\right)(2\pi r \sin\theta_1) r\,\mathrm{d}\theta_1$$

$$= 0{\cdot}682. \tag{27}$$

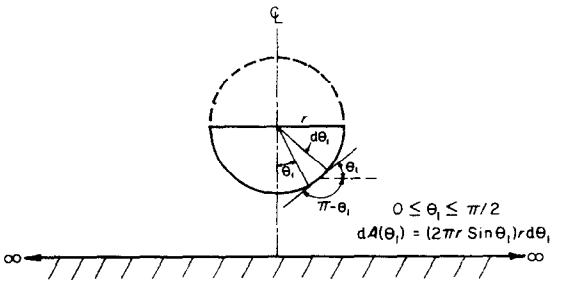

FIG. 3. Configuration factor for thermal radiation from infinite surface to a lower hemisphere.

Similarly, by the geometrical configuration presented in Fig. 4 the value for $\bar{F}_2$ is found to be

$$\bar{F}_2 = \frac{1}{A_2}\int \frac{2(\pi/2 - \theta_2)}{2\pi}\,\mathrm{d}A_2$$

$$= \frac{1}{2\pi r^2}\int_0^{\pi/2}\left(\frac{\pi/2 - \theta_2}{\pi}\right) 2\pi r \cos\theta_2 r\,\mathrm{d}\theta_2$$

$$= 0{\cdot}318. \tag{28}$$

Substituting equation (27) into equation (25) and then into equation (23), the radiation heat transfer between the plate and the lower half of the droplet is

$$Q_{R1} = \frac{A_1\sigma(T_P^4 - T_S^4)}{[(1/\varepsilon_L) - 1] + 1/0{\cdot}682}. \tag{29}$$

Similarly, the radiative heat transfer between the plate and the upper half of the droplet is

$$Q_{R2} = \frac{A_2\sigma(T_P^4 - T_S^4)}{[(1/\varepsilon_L) - 1] + 1/0{\cdot}318}. \tag{30}$$

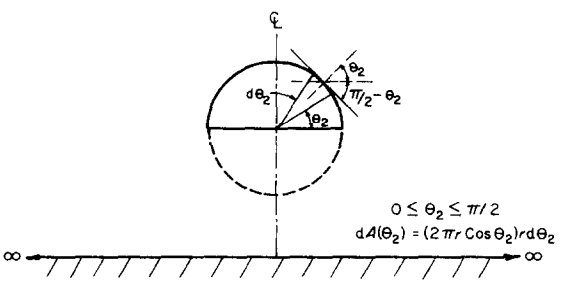

FIG. 4. Configuration factor for thermal radiation from infinite surface to an upper hemisphere.

With equations (2), (21), (22), (29), and (30), the effective heat transfer from the plate to the bottom half of the droplet, Q_1 is:

$$Q_1 = \frac{k_e \Delta T}{\delta} A_p$$

$$= Q_c + Q_{R1} + Q_{R2} - W_2\lambda \quad (31)$$

where $k_e = (1 + K)k$.

K is defined as the correction factor between the actual thermal conductivity of vapor, k and the effective thermal conductivity for the heat transfer taking place between the heating plate and the lower half of droplet, k_e. In computation, K is first set equal to 0 and then consecutively approximated by $K = Q_{R1}/Q_c$. The convergence of K is checked by equation (31).

It is seen from the above analysis that the final form of equation (1) is very nonlinear. This nonlinearity precludes an analytical solution for the total evaporation time and evaporation rate of droplets in the Leidenfrost regime, and a numerical analysis was developed.

A functional analysis gives the following equation:

$$\frac{dV}{dt} = -\frac{1}{\rho_L}(W_1 + W_2) = f(V, t). \quad (32)$$

This type of first order, ordinary differential equation may be appropriately solved by using the modified Euler's method [16]. The computational details are given in reference [17] and will not be developed here.

3. EXPERIMENTAL PROCEDURE

The experimental apparatus is shown schematically in Fig. 5. The test surface was a Type 304 stainless steel plate centered and resting on a flat wire-wound electric resistance element; complete plate dimensions are given in Fig. 6. Five 24 gauge Chromel–Alumel thermocouples were installed $\frac{1}{16}$ in below the test surface and cemented to the plate with sauereisen high-temperature cement. The surface of the plate was polished to a mirror finish; after heating to operating temperature for about an hour, the surface developed a golden brown color without losing its smoothness. The electric resistance element was a 14-in × 8 in $\frac{3}{4}$-Hevi-Duty #56-TS unit. The resistance element heat output was controlled by a 10-A 120-V Variac connected to the 120-V 60-cycle laboratory power. The thermocouple output was read on a Leeds and Northrup #8690 millivolt potentiometer.

A Konica FS 35-mm still camera with an

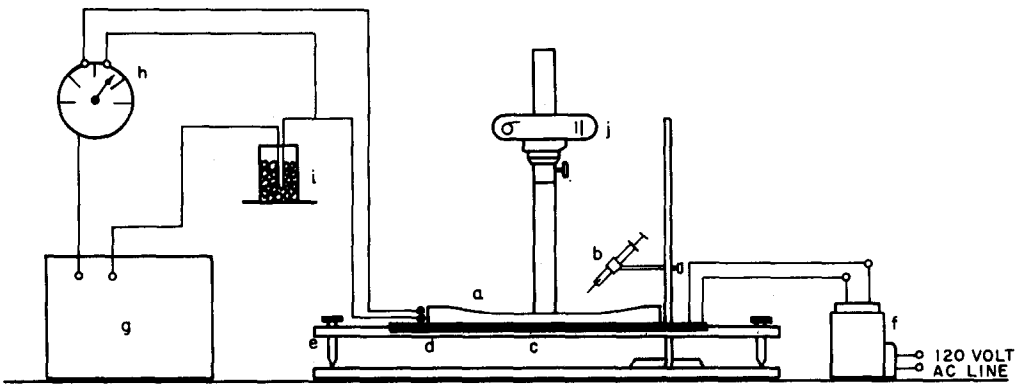

FIG. 5. Schematic of apparatus.

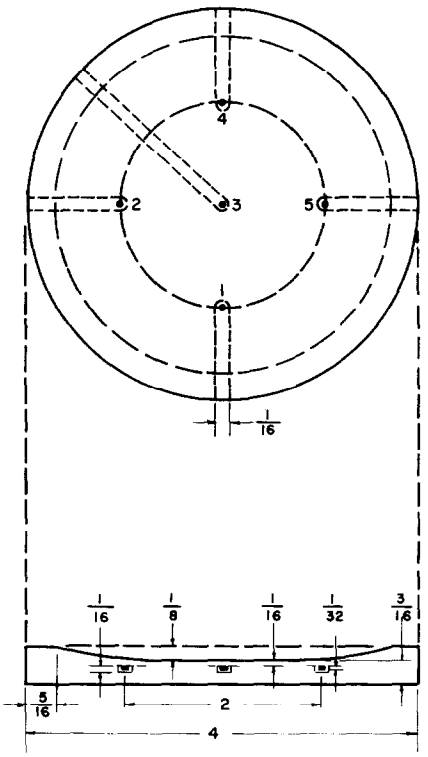

FIG. 6. Diagram of stainless steel plate (dimensions in inches).

Ednalite +3 close-up lens was mounted on a photographic copying stand and used to photograph droplets during evaporation.

The liquid droplets were produced with a hypodermic syringe with 13-, 16-, 17-, and 21-gauge stainless-steel needles. The needles were filed to a smooth flat tip. The syringe and needle were fixed in a stand at a 45° angle to the horizontal with the needle tip about $\frac{1}{2}$ in above the plate near the edge. This placed the body of the syringe and most of the needle in the ambient atmosphere. The syringe plunger was slowly screwed down and a droplet formed on the needle tip until the droplet weight became sufficient to detach from the tip. All needles were calibrated for droplet size at room temperature with each liquid by forming and individually weighing ten droplets in a narrow-necked bottle. Mean deviation was ±2·9 per cent from the arithmetic mean for the worst case (carbon tetrachloride) and ±1·1 per cent for water. A similar calibration was made at about the boiling temperature for each liquid and gave drop sizes about 10 per cent smaller.

The test liquids were:

Water: Distilled; no detectable impurities; b.p. 100·0°C.

Benzene: Reagent; purity from gas chromatography 99·6 per cent; b.p. 80·1°C, boiling range 0·3°C (1 ml–95 ml), 0·4°C (95 ml-dryness).

Carbon tetrachloride: Reagent; purity from chromatograph 99·3 per cent; b.p. 76·7°C, boiling range 0·2°C (1 ml–95 ml), 0·1°C (95 ml–dryness).

Ethanol: Reagent; purity from chromatograph 99·7 per cent; b.p. 78·5°C.

n-Octane: Research Grade: purity from chromatograph 99·2 per cent, b.p. 125·8°C.

For each series of runs, the Variac was set at a fixed value and the test plate heated up. The plate would reach steady state in two to four hours; maximum variation between thermocouple readings was 2 degC. The syringe was filled with liquid and mounted. Droplets were formed as noted before. The time required for a given droplet to evaporate completely after hitting the plate was measured with a stop watch readable to 0·01 s. If the droplet shattered upon hitting the plate, picked up dirt, bounced vertically at any time during the evaporation, or wandered off the test surface, the run was rejected. Care was taken to keep the plate clean during the test and to minimize all external air currents. At least three separate vaporization time determinations were made for each set of experimental conditions—more if there were a difference in evaporation time of ±0·5 s or ±1 per cent from the mean.

To study the instantaneous droplet size during evaporation, several runs were made in which still photographs were taken of the droplet at carefully measured 5–10-s intervals. Camera settings were *f*2 at $\frac{1}{1000}$ s using Kodak Tri-X film (ASA rating 400) and a Woolensak WF-36

Xenon Lamp for lighting. Each frame of the film was developed and mounted in a slide. The droplet diameter was measured using a $\times 320$ precision metallurgical microscope with a micrometer drive on the object deck. The micrometer drive was calibrated to $\pm 0{\cdot}001$ cm using an optical micro-scale and true droplet size was established by two steel scales placed on the plate.

4. RESULTS AND DISCUSSION

The experimental total vaporization time results are shown in Figs. 7–11. The mean points are plotted and the range of experimental results indicated by the vertical bar. The temperature difference which gives maximum evaporation time is presumed to be the minimum temperature at which stable film boiling can exist and is termed the Leidenfrost point. To the left of the Leidenfrost point, the boiling is in the transition regime between nucleate and film. The Leidenfrost point is not a strong function of size, as has been noted over a much wider size range in reference [18]. These results are in good agreement with the more limited data reported in reference [12] and the extensive results in reference [14].

There is considerable difference of opinion as to the exact temperature of the Leidenfrost point for water. The transition regime is much wider for water than for the other liquids; this has been noted many times in pool boiling experiments as well as in Leidenfrost work. The problem is discussed at some length in reference [18]; in general we may say that the value of the Leidenfrost point for water depends

(1) strongly upon the surface material, generally but not necessarily increasing as the thermal diffusivity of the surface decreases,

and

(2) weakly upon the initial water temperature, decreasing as the initial water temperature increases.

The problem seems to be primarily one of hot surface temperature transients rather than any intrinsic change in the Phenomenon itself. The fact that this variation in the Leidenfrost temperature is so much more evident for water than for organics is probably due to the greater latent heat of water. A study of this problem is being made.

The theoretical predictions for total evaporation time obtained from the analysis in this paper are shown for the largest and smallest

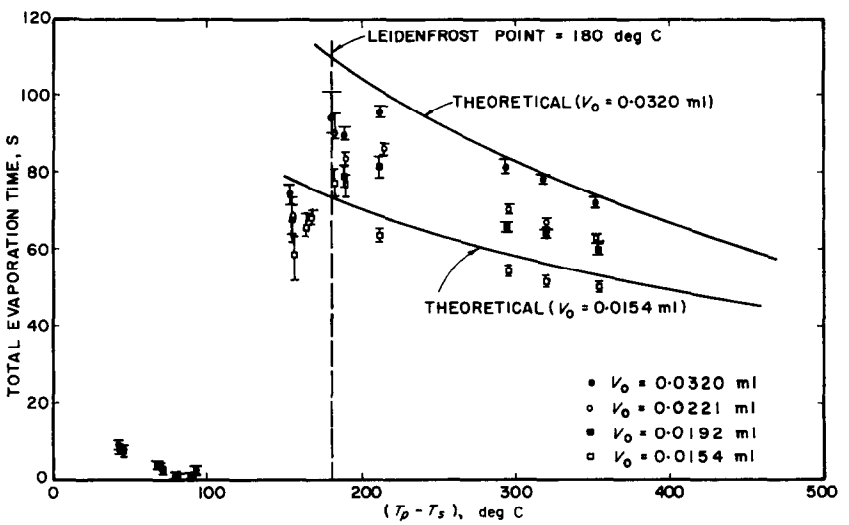

FIG. 7. Total evaporation time vs. ΔT for water droplets.

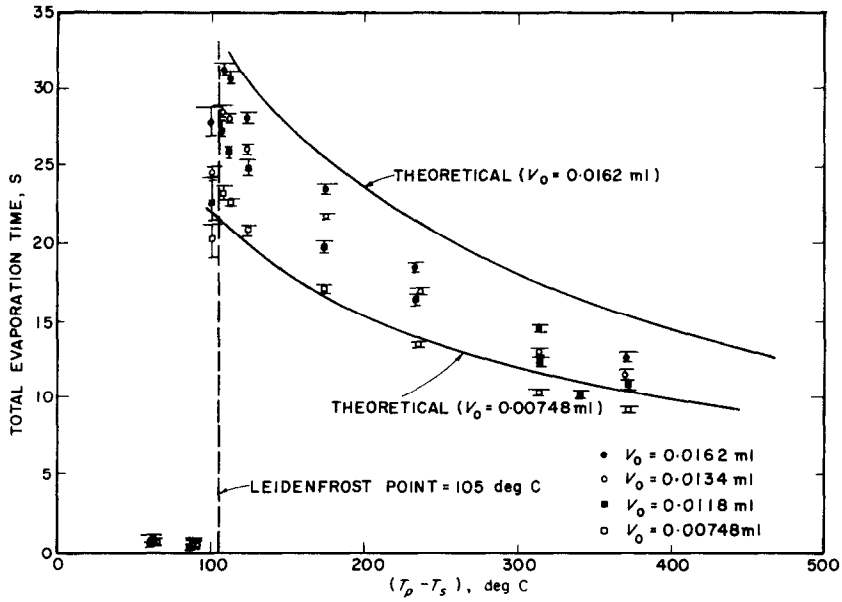

FIG. 8. Total evaporation time vs. ΔT for benzene droplets.

drop sizes of each liquid tests. Similar curves for the intermediate sizes are given in reference [17], but are omitted here to reduce confusion. The theoretical results are seen to be in fair agreement with experiment except for *n*-octane. The analysis in reference [14] predicts evaporation times 10–35 per cent lower than the present analysis.

For *n*-octane reference [12] establishes that thermal cracking occurs for plate temperatures above about 250°C with about 20 per cent decomposition occurring at 460°C. Over this temperature range, approximately half (by weight) of the cracked products polymerize to form heavier-than-*n*-octane gases. Marschner [19] has also reported *n*-octane cracking on

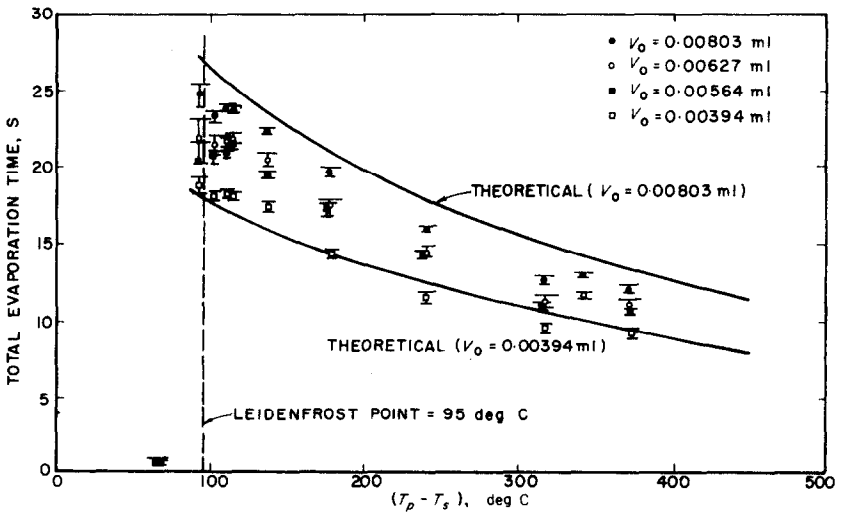

FIG. 9. Total evaporation time vs. ΔT for carbon tetrachloride droplets.

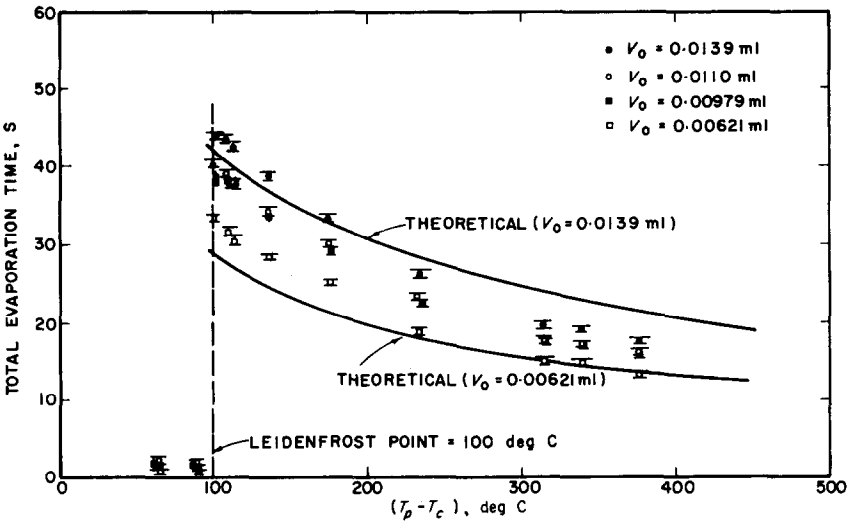

FIG. 10. Total evaporation time vs. ΔT for ethanol droplets.

stainless steel in the 200–600°C range. The effect of cracking on evaporation rate is complex: The cracked products have higher thermal conductivity and lower viscosity than the octane, but the cracking reaction is endothermic and there is an increase in gas volume to flow out. The opposite effects obtain for the polymerization reaction.

Another test for evaluating the theoretical model is found in the comparison of the photographic data on the instantaneous droplet size and the theoretically predicted values. The instantaneous radii from photographic measurements are presented for two cases in Figs. 12 and 13. The solid points represent the average experimental data obtained from direct microscopic

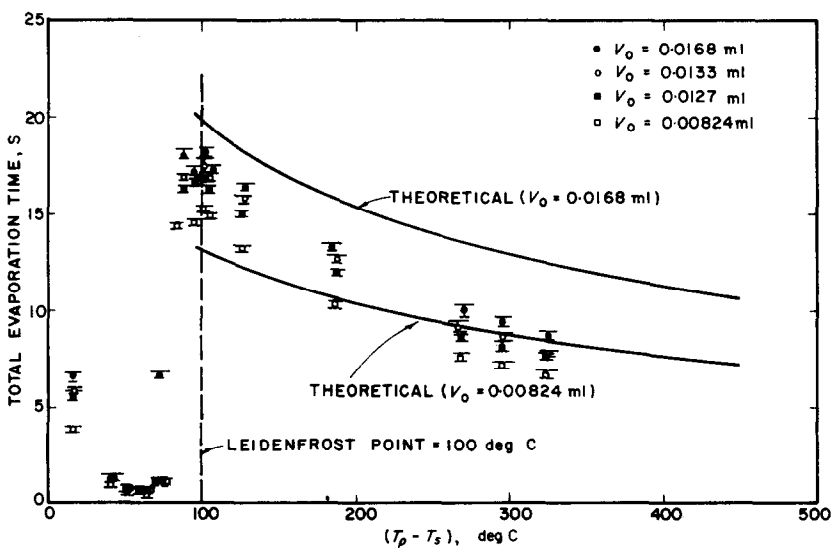

FIG. 11. Total evaporation time vs. ΔT for *n*-octane droplets.

measurements on the film slides. The uncertainties of these measurements are indicated by two bars which give the range of variation. The "normalized" points were obtained by shifting the time scale so that the droplet would appear to totally evaporate in the time predicted by the theory. The examples shown are indicative of the results of a number of such tests, Fig. 12 showing close agreement with the analytical model and Fig. 13 showing about the poorest agreement found. In general the water and carbon tetrachloride results showed the best

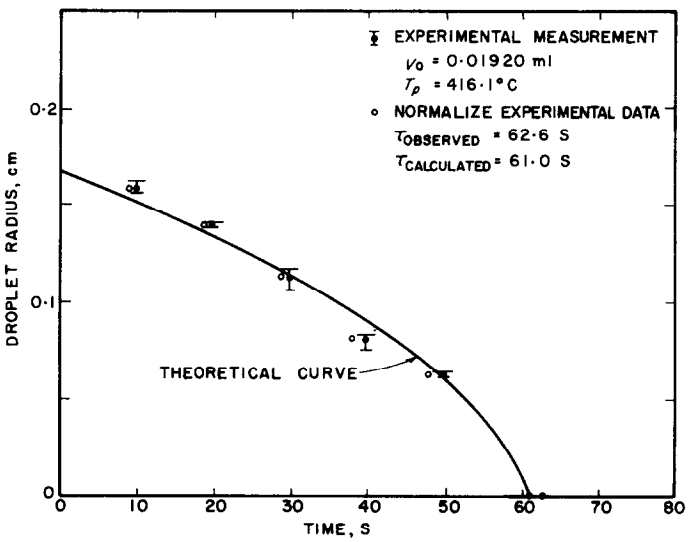

FIG. 12. Droplet radius vs. time; water droplet.

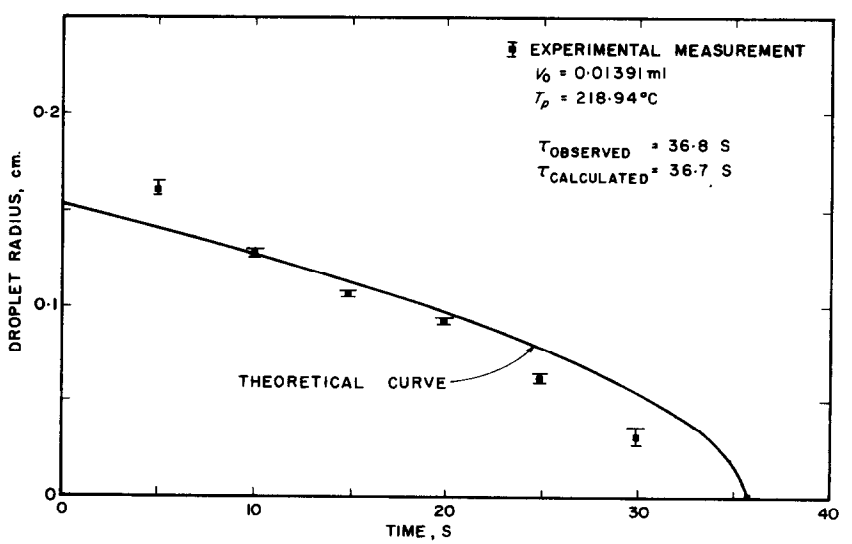

FIG. 13. Droplet radius vs. time; ethanol droplet.

agreement with theory and benzene and ethanol the poorest. No tests of this kind were made for octane.

One assumption of the analytical development that should be examined here is that of sphericity of the droplets. Bashforth and Adams [20] described droplet shapes (in a uniform pressure field except at the surface of support) as a function of volume, density, and surface tension and constructed a table to indicate the degree of deviation from sphericity by using the dimensionless group $(\rho_L g r^2/\bar{\sigma})$ as parameter. The deviation from sphericity is defined as the ratio of the major to the minor radius. For a perfect sphere, this ratio is unity. If we accept a ratio of 1·10 as a criterion of essential sphericity, the dimensionless group $(\rho_L g r^2/\bar{\sigma})$ must be equal to or less than 0·57. The values for the droplets used in this work are shown in Table 1 and it is seen that the assumption holds best for water and poorest for octane and carbon tetrachloride. For the largest octane droplet, the diametral ratio is 1·17. The criterion is not exact because the droplets are supported somewhat differently in the Bashforth and Adams analysis.

Table 1. Dimensionless criterion for droplet sphericity

Liquid	Droplet volume ml	$g\rho_L r^2/\bar{\sigma}$
CCl_4	0·00803	1·1603
	0·00627	0·9183
	0·00394	0·7213
C_2H_5OH	0·01391	0·9663
	0·01100	0·7610
	0·00621	0·5606
C_6H_6	0·01618	0·9673
	0·01343	0·7840
	0·00748	0·5792
H_2O	0·03196	0·6337
	0·02212	0·4498
	0·01540	0·3129
n-C_8H_{18}	0·01682	1·1956
	0·01266	0·9903
	0·00824	0·7428

Calculated values of the droplet volume V, radius, r, and the vertical distance from bottom of droplet to plate, δ_1, are shown in Fig. 14 as functions of droplet lifetime for a water droplet on a 500°C plate. It may be seen that in this case δ_1 is less than about 0·002 cm, which is typical of all of the droplets considered in this study. There was no experimental measurement for the magnitude of δ_1 in this work. Kistemaker [10]

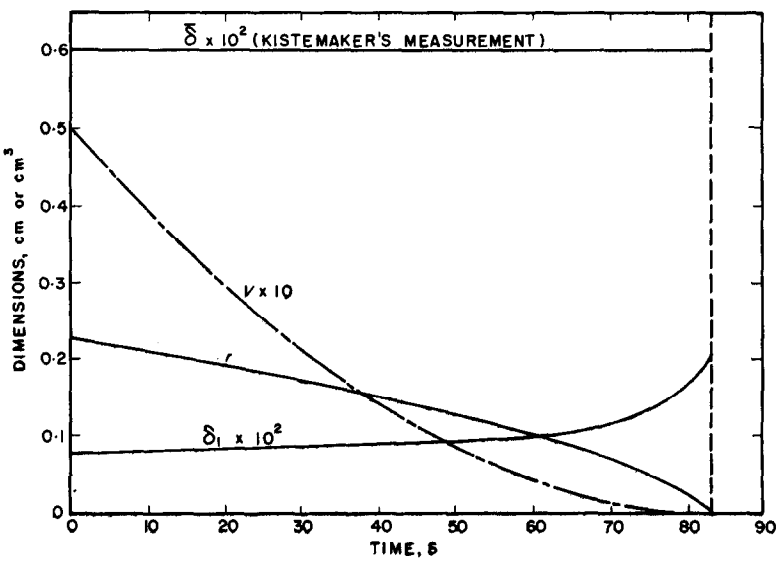

FIG. 14. Calculated history of droplet dimensions; water droplet at T_P = 500°C. (V_0 = 0·05 ml).

measured the vapor film thickness of 0·006 cm for a water droplet at $T_P = 500°C$ from his X-ray photographs. Instead of allowing the droplet to have complete freedom of motion on the hot surface, Kistemaker as well as Gorton [13] confined the liquid droplet at the tip of a delivering pipet. This technique has the advantage of keeping the droplet at constant volume and in one place. However, the droplet is then partially supported by surface tension and a different force balance is required. Kistemaker's measurement technique also tends to give a vapor layer thickness rather larger than the minimum. We may say that Kistemaker's result differs from ours in a qualitatively expectable fashion but cannot be considered to verify the present theory.

The Reynolds number for the radial flow of vapor beneath the droplet is shown in Fig. 15 for water at $T_P = 280°C$ and 500°C. Calculations carried out for the other liquids show that the Reynolds number never exceeds 16 for the range of this study. The assumption of laminar flow of the vapor is supported by these results.

Figure 16 shows the heat flux history of water droplets at $T_P = 280°C$ and $T_P = 500°C$ as obtained from the theoretical computation. At the higher plate temperature, the radiative heat flux is about 60 per cent of the conductive–convective heat flux; at the lower plate temperature, the radiative flux is only about 30 per cent of the conductive–convective flux.

The rates of evaporation per unit area from the lower and upper halves of the droplet, W_1/A_1 and W_2/A_2, are plotted as a function of time in Fig. 17 for water droplets at 280°C and 500°C plate temperature respectively. It appears that at higher temperatures, the evaporation rate from the lower half of the droplet predominates over the molecular diffusion from the upper half of droplet; at lower plate temperatures, the evaporation due to molecular diffusion W_2/A_2 becomes relatively more important than W_1/A_1, especially towards the end of droplet evaporation.

In Figs. 14–17, the calculated history is given for a droplet of 0·05-ml initial volume. However, the curves should also apply to any smaller initial volume at the same plate temperature if one starts at a point on the curve such that the

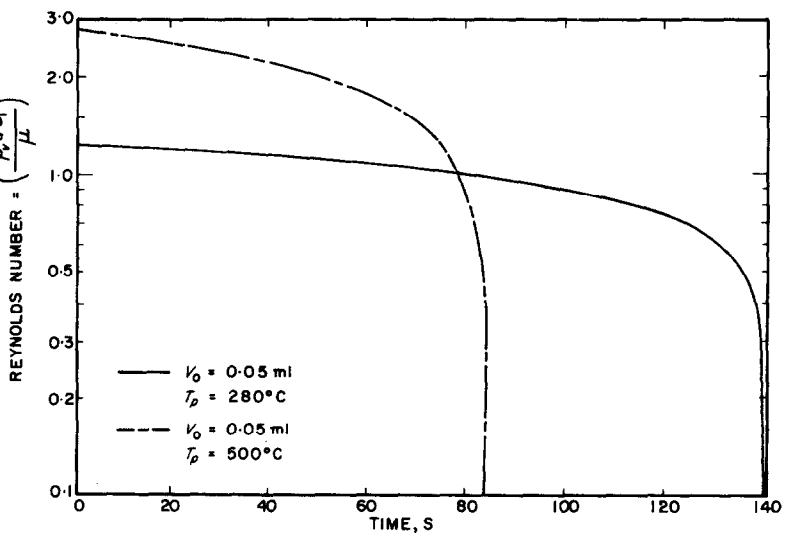

FIG. 15. Calculated Reynolds number vs. time for water droplets.

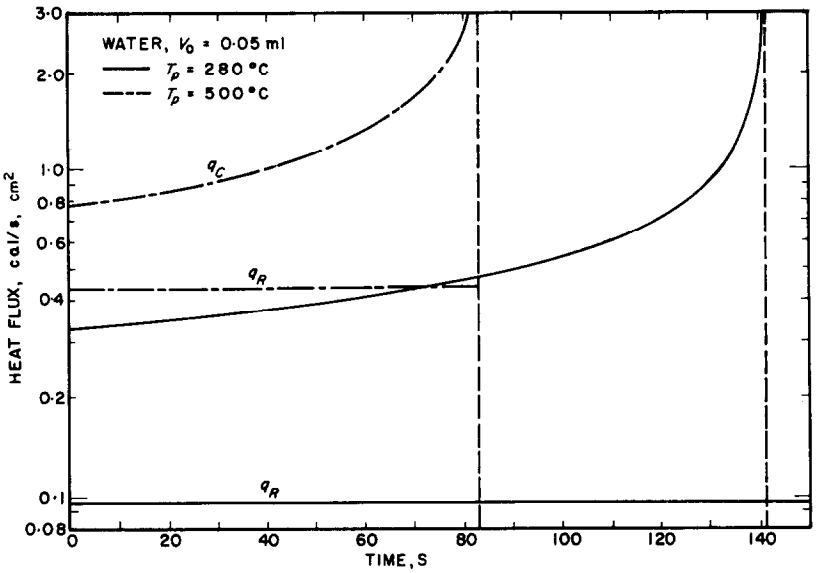

FIG. 16. Calculated heat-flux history of water droplets.

remaining time to total evaporation is equal to the total evaporation time of the droplet size in question.

Thus, for $V_0 = 0{\cdot}0154$ at $T_P = 500°C$, total evaporation time is seen to be about 83 − 38 = 45 s from Fig. 14 (or a similar value from the experimental results in Fig. 7) and corresponding values are $r_0 = 0{\cdot}15$ cm and $\delta_1 = 0{\cdot}0009$ cm.

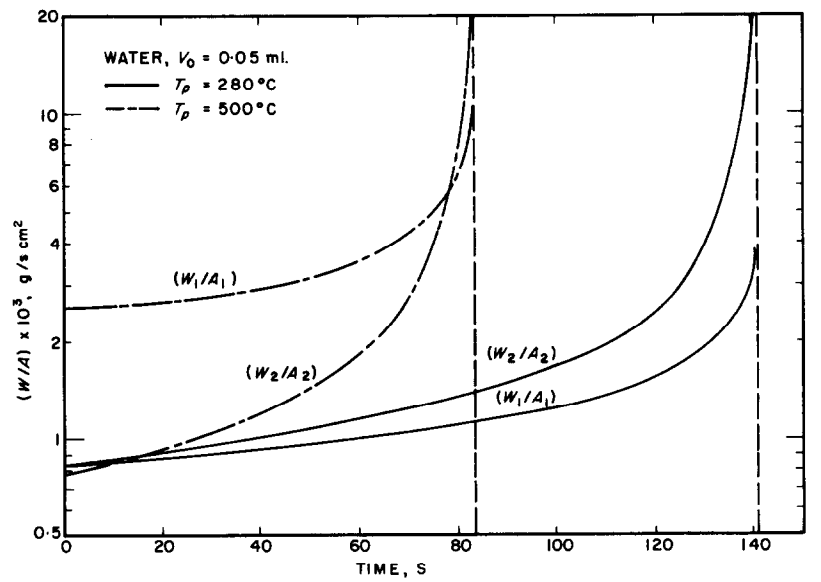

FIG. 17. Calculated evaporation rates vs. time for water.

5. ENGINEERING CORRELATION

The development in Section 2 is purely analytical. It does not require any experimental data (except physical properties) in the prediction for droplet evaporation time; however, it involves complicated iterative computations before it converges to the correct values for droplet evaporation time. Thus, a digital computer is a necessary tool. For engineering calculation, it is desirable to obtain a relatively simple equation which would imply the correct functional dependence upon variables and allow a prediction for droplet evaporation time without recourse to a computer. In order to obtain such an empirical correlation of the experimental data, a functional equation between the dependent variable and the independent variables must be obtained.

From the theoretical development, we find that heat is transferred from the plate to the droplet by conduction and radiation, neither one of which may be neglected in general. The evaporation rate per unit area for a spherical droplet is on the order of $\rho_L r_0/\tau$ and this quantity is equal to the sum of the heat transferred by conduction and radiation divided by λ'. Functional arguments are developed in detail in reference [17], but the resulting equation is

$$\frac{\rho_L r_0}{\tau} = C_1\left[\frac{k\,\Delta T\, r_0 g \rho_V(\rho_L - \rho_V)}{\mu\lambda'}\right]^{\frac{1}{4}} + C_2\left[\frac{\sigma\varepsilon_P(T_P^4 - T_S^4)}{\lambda'}\right], \quad (33)$$

where C_1 and C_2 are constants to be evaluated from the experimental data.

Seventy-two data points representing the full range of experimental conditions were selected and used to calculate C_1 and C_2 by least squares fitting. The result is

$$\frac{\rho_L r_0}{\tau} = 1{\cdot}17 \times 10^{-2}\left[\frac{k\,\Delta T r_0 g \rho_V(\rho_L - \rho_V)}{\mu\lambda'}\right]^{\frac{1}{4}} + 2{\cdot}38\left[\frac{\sigma\varepsilon_P(T_P^4 - T_S^4)}{\lambda'}\right]. \quad (34)$$

The correlation is shown in Fig. 18 for the test

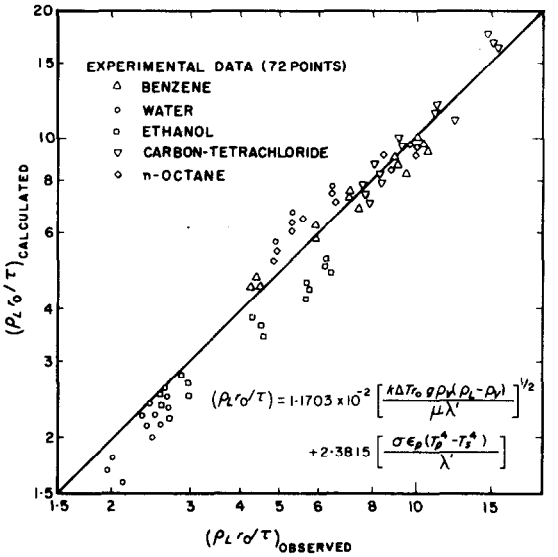

FIG. 18. Empirical correlation of total evaporation time.

points. The average error is about ±20 per cent.

Borishansky [12] has correlated his data for spherical droplets by plotting

$$\frac{k_L\tau}{2C_L\rho_L r_0}\sqrt{\left[\frac{(\rho_L - \rho_V)}{\bar{\sigma}}\right]}$$

against

$$\frac{C_L(T_P - T_S)}{\bar{\lambda}}\frac{k_V}{k_L}$$

for the four fluids considered. The quantities in the dimensionless groups are those quantities which are parameters in Borishansky's mechanistic model. (Note the appearance of the thermal conductivity of the liquid, k_L, the heat capacity of liquid, C_L, and the liquid interfacial tension, $\bar{\sigma}$. These parameters do not enter the analytical model developed herein.) The data presented by Borishansky all fall along a curve with an average error of about ±20 per cent. By plotting the inverse of the ordinate against the abscissa, however, it is seen that, for

$$\frac{C_L(T_P - T_S)}{\lambda}\frac{k_V}{k_L} < 0{\cdot}10,$$

the data fall on a straight line through the origin (cf. Fig. 19). This causes k_L and C_L to drop out, resulting in

$$\frac{\rho_L r_0}{\tau}\sqrt{\left[\frac{\bar{\sigma}}{(\rho_L-\rho_V)}\right]} = 16{\cdot}7\left(\frac{k_V\,\Delta T}{\lambda}\right). \quad (35)$$

For $\rho_L \gg \rho_V$, equation (35) simplifies to

$$\frac{r_0\sqrt{(\bar{\sigma}\rho_L)}}{\tau} = 16{\cdot}7\left(\frac{k_V\,\Delta T}{\lambda}\right). \quad (36)$$

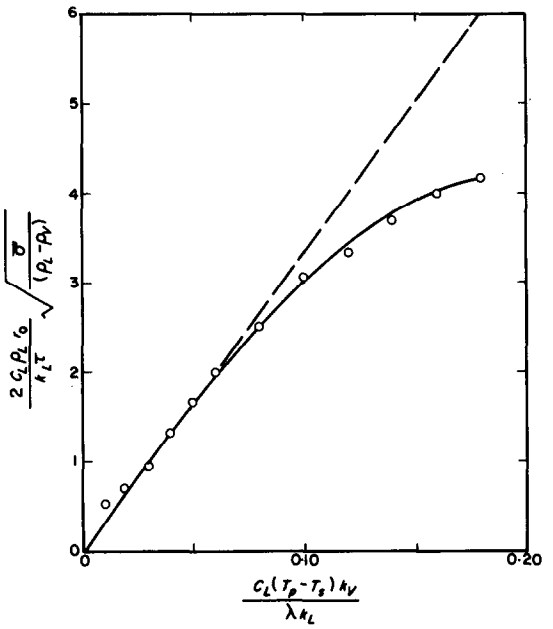

FIG. 19. Borishansky correlation.

Gottfried [14] developed a similar correlation by applying dimensional analysis to averaged sets of the data presented in reference [14]. The resulting correlation is

$$\tau\sqrt{\left(\frac{g}{r_0}\right)} = 37{\cdot}8\left(\frac{k_V\,\Delta T}{\rho_V D\lambda}\right)^{-0{\cdot}735} \times\left(\frac{\rho_L}{\rho_V}\right)^{0{\cdot}407}\left(\frac{C_p\mu}{k_V}\right)^{-0{\cdot}874}\left(\frac{\mu}{\rho_V D}\right)^{0{\cdot}714} \times\left[\frac{D}{\sqrt{(gr_0^3)}}\right]^{-\frac{1}{4}} \quad (37)$$

This correlation is shown graphically in Fig. 20. Although equation (37) is more complicated

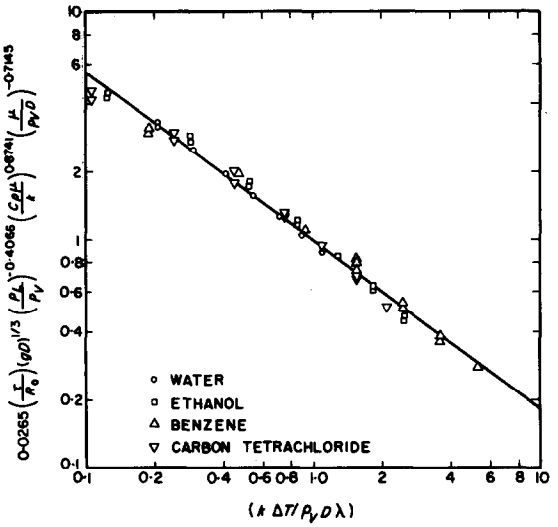

FIG. 20. Gottfried correlation.

than equations (34)–(36), the average error in its use is less than ±10 per cent. The correlation only applies, however, for

$$0{\cdot}10 \leqslant \left(\frac{k_V\,\Delta T}{\rho_V D\lambda}\right) \leqslant 5{\cdot}0,$$

$$300 \leqslant \left(\frac{\rho_L}{\rho_V}\right) \leqslant 4000,$$

and for $(C_p\mu/k)$ and $(\mu/\rho_V D)$ approximately equal to one.

6. CONCLUSIONS

(1) The proposed theoretical model is supported reasonably well by the experimental data taken with small droplets of ordinary liquids.
(2) The major contribution to the heat transfer is the conductive–convective mechanism.
(3) The radiative heat flux cannot be neglected at plate temperatures beyond the Leidenfrost point of liquids.
(4) The radial flow of vapor beneath the droplet is laminar.
(5) The Leidenfrost point is well defined for organic liquids, while for water it is between 250°C and 310°C plate temperature.

(6) The Leidenfrost point is found to be essentially independent of droplet size for the range of droplet volumes studied.
(7) Data are well-correlated, allowing prediction of total vaporization time to within ± 20 per cent.

7. FURTHER WORK

Additional studies have recently been completed or are currently under way on the following topics:

(1) The Leidenfrost phenomenon for extended liquid masses, such that the liquid mass flattens out and at still larger sizes permits vapor bubbles to break through the mass.
(2) The Leidenfrost phenomenon for two-component solutions.
(3) The Leidenfrost phenomenon for cryogenic fluids.
(4) The role played by heating surface conditions at the Leidenfrost point.
(5) The Leidenfrost phenomenon for *n*-octane, to ascertain the cause of its apparently anomalous behavior, and other ordinary liquids.

ACKNOWLEDGEMENTS

Financial support and equipment funds for the initial phases of this work were gratefully received from the Office of Engineering Research of Oklahoma State University; The U.S. Army Research Office (Durham, North Carolina) supported the research entirely during the last two years of this work. The Wollensak Xenon Lamp used as the light source in the photographic study was purchased with a grant from the National Science Foundation. Phillips Petroleum Company supplied *n*-octane for this work and also generously donated time on their IBM 7094 computer for part of the computation in this work.

Graduate Fellows B. M. Patel and E. S. Godleski assisted with the experimentation and made numerous helpful suggestions. Mrs. Arleen Fairchild typed the manuscript.

REFERENCES

1. J. G. LEIDENFROST, *De Aquae Communis Nonnullis Qualitatibus Tractatus, (A Tract About Some Qualities of Common Water)*, Duisburg on Rhine (1756). An original copy of this Treatise is in the Yale University Library.
2. C. WARES, DeGolyer Collection in the History of Science and Technology, University of Oklahoma (1963).
3. B. THOMPSON (COUNT RUMFORD), *Phil. Trans. R. Soc.* **94**, 77–182 (1804).
4. J. C. POGGENDORFF, *Ann. Phys.* **52**, 497 (1841).
5. J. STARK, *Ann. Phys.* **65**, 306 (1898).
6. P. M. BOUTIGNY, *Annali Chim.* **9**, 350–370 (1843).
7. J. L. PARTINGTON, *Advanced Treatise on Physical Chemistry*, Part II, 282–283. Longman, Green, London (1951).
8. L. GMELIN, *Hand-book of Chemistry*, Part I (Translated by H. WATTS), 277–278. Harrison, London (1848).
9. J. BERGER, *Annln Phys.* **119**, 594 (1863).
10. J. KISTEMAKER, *Physica,'s Grav.* **29**, 96–104 (1963).
11. N. A. PLETENEVA and P. A. REBINDER (Russian), *J. Phys. Chem.* **20**, 961–972 (1946).
12. V. M. BORISHANSKY, AEC Trans. Series, AEC-TR-3405 (1953).
13. C. W. GORTON, Ph.D. Thesis, Purdue University (1953).
14. B. S. GOTTFRIED, Ph.D. Thesis, Case Institute of Technology (1962).
15. MCADAMS, *Heat Transmission*, 3rd Edition. McGraw-Hill, New York (1954).
16. K. S. KUNZ, *Numerical Analysis*. McGraw-Hill, New York (1957).
17. C. J. LEE, Ph.D. Thesis, Oklahoma State University (1965).
18. B. M. PATEL, Ph.D. Thesis, Oklahoma State University (1965).
19. R. F. MARSCHNER, *Ind. Engng Chem.* **30**, 554–562 (1938).
20. F. BASHFORTH and J. C. ADAMS, *An Attempt to Test the Theory of Capillary Action*, University Press, Cambridge (1883).
21. J. DAVISON, Senior Report, Oklahoma State University (1965).

Résumé—L'ébullition par film de petites gouttelettes de liquides sur une surface plane chauffée dans l'atmosphère est appelée habituellement le phénomène de Leidenfrost d'après J. G. Leidenfrost qui étudie le premier ce processus en 1756.

Dans l'étude actuelle, on a déterminé les temps d'évaporation totale pour de petites gouttelettes (0, 1 ml) d'eau, de tétrachlorure de carbone, d'éthanol, de benzène et de *n*-octane sur une plaque d'acier inoxydable avec des températures pariétales allant de 150°C à 500°C. La plupart des données expérimentales correspondent au régime d'ébullition par film bien que d'autres résultats correspondent aux régimes d'ébullition nucléée et de transition. Le point de Leidenfrost, défini comme la température de la plaque pour laquelle le temps d'évaporation de la gouttelette est le plus grand, a été déterminé. On a trouvé que le point de Leidenfrost est entre 100 à 105degC au-dessus de la température de saturation pour tous les liquides excepté l'eau; pour l'eau, la valeur exacte du point de Leidenfrost semble dépendre de la surface et de la

façon de déposer la gouttelette et varie entre 150degC à 210degC audessus de la saturation. Le point de Leidenfrost est indépendant de la taille de la gouttelette dans la gamme étudiée.

On a imaginé un modèle théorique du phénomène de Leidenfrost: la chaleur est transportée à la gouttelette par conduction à travers le film de vapeur sur la moitié inférieure et par rayonnement à la gouttelette toute entière.

De la masse est enlevée de la gouttelette par évaporation sur la surface inférieure pour nourrir le film de vapeur et par diffusion à partir de la surface supérieure. La gouttelette est soutenue par la pression supplémentaire dans le film de vapeur. On a supposé que la gouttelette est sphérique et isotherme à la température de saturation. La vitesse instantanée d'évaporation est obtenue en satisfaisant aux bilans de chaleur, de masse et de quantité de mouvement pour ce modèle; les temps d'évaporation totale sont calculés en intégrant la vitesse d'évaporation. Les temps d'évaporation calculés et expérimentaux sont en accord à 20 pourcent prèssauf pour le *n*-octane aux températures élevées, où il se peut qu'il se produise un certain craquage thermique.

Zusammenfassung—Das Filmsieden kleiner Flüssigkeitströpfchen auf einer heissen, ebenen Fläche in der Atmosphäre wird gewöhnlich Leidenfrostphänomen genannt nach J. G. Leidenfrost, der den Vorgang 1756 als erster studierte.

In der vorliegenden Untersuchung werden Gesamtverdampfungszeiten für kleine Tröpfchen (<0,1 ml) aus Wasser, Kohlenstofftetrachlorid, Äthanol, Benzin und *n*-Oktan auf einer (stainless) Stahlplatte bei Oberflächentemperaturen von 150°C bis 500°C bestimmt. Die Mehrzahl der Daten wurde im Bereich des Filmsiedens gewonnen, daneben aber auch im Blassen- und Übergangssiedebereich. Der Leidenfrostpunkt, definiert als die Plattentemperatur, bei der die Verdampfungszeit der Tröpfchen am grössten ist, wurde bestimmt. Der Leidenfrostpunkt lag 100–105 deg über der Sättigungstemperatur für alle Flüssigkeiten ausser Wasser; für Wasser scheint der genaue Wert des Leidenfrostpunktes von der Oberfläche abzuhängen und der Art der Tropfenaufbringung und er variiert von 150 bis 210 deg oberhalb der Sättigung. Der Leidenfrostpunkt ist unabhängig von der Tröpfchengrösse im untersuchten Bereich.

Ein analytisches Modell des Leidenfrostphänomens wurde aufgestellt: Wärme wird auf das Tröpfchen übertragen durch Leitung durch den Dampffilm an Bodenhälfte und durch Strahlung an den ganzen Tropfen. Der Stofftransport vom Tropfen erfolgt durch Verdampfen an der unteren Oberfläche, um den Dampffilm aufrechtzuerhalten und durch Diffusion an der oberen Oberfläche. Dan Tröpfchen wird getragen durch den Überdruck im Dampffilm. Der Tropfen wird kugelig und isotherm mit Sättigungstemperatur angenommen. Die momentane Verdampfungsgeschwindigkeit wird auf Grund der Wärme-, Stoff- und Impulsbilanz für dieses Modell gefunden; Gesamtverdampfungszeiten werden durch Integration der Verdampfungsgeschwindigkeit berechnet. Die Übereinstimmung der berechneten und der experimentallen Verdampfungszeiten liegt innerhalb 20 Prozent, ausgenommen *n*-Oktane bei hohen Temperaturen, wobei bereits thermische Crackerscheinungen aufgetreten sein können.

Аннотация—Пленочное кипение мелких капель жидкости на горячей плоской поверхности в атмосфере обычно называется эффектом Лейденфроста в честь открывшего и изучившего его Дж. Г. Лейденфроста (1756 г).

В данной работе общее время испарения определялось для небольших капель (< 0,1 мл) воды, четыреххлористого углерода, этанола, бензина и *n*-октана на пластине из нержавеющей стали при температурах поверхности от 150 до 500°C. Большинство результатов относится к режиму пленочного кипения, хотя также были получены данные в режимах пузыркового и нестационарного кипения. Была найдена точка Лейденфроста, определяемая как температура пластины, которой соответствует наибольшее время испарения. Она была на 100–105°C выше температуры насыщения для всех жидкостей за исключением воды. Для воды точное значение точки Лейденфроста оказалось зависящим от поверхности и способа нанесения капель и было на 150–210°C выше температуры насыщения. Точка Лейденфроста не зависит от размера капель во всем диапазоне измерений. Принимается следующая модель эффекта Лейденфроста: тепло переносится к капле теплопроводностью через пленку пара в нижней половине капли и излучением ко всей капле. Вещество удаляется из капли испарением в нижней части капли, создавая при этом паровую пленку, и диффузией с верхней. Капля поддерживается во взвешенном состоянии за счет избыточного давления в паровой пленке. Форма капли считается шарообразной, и при температуре насыщения идет изотермический процесс. Мгновенная скорость испарения для этой модели найдена путем удовлетворения уравнений баланса тепла, массы и количества движения. Продолжительность испарения вычислена интегрированием скорости испарения. Расчетное

и экспериментальное значение времени испарения согласуются между собой с точностью до 20 процентов, за исключением *n*-октана при высоких температурах, когда может происходить термический крекинг.